Spatiotemporal Dynamics of Wormlike Micelles under Shear

Lydiane Bécu,* Sébastien Manneville, and Annie Colin†
Centre de Recherche Paul Pascal, Avenue Schweitzer, 33600 Pessac, France
(Received 5 February 2004; published 28 June 2004)

Velocity profiles in a wormlike micelle solution (cetyl trimethyl ammonium bromide in D_2O) are recorded using ultrasound every 2 s during a startup experiment into the shear-banding regime. The stress relaxation occurs over more than 6 h and corresponds to the very slow nucleation and growth of the high-shear band. Moreover, oscillations of the interface position with a period of about 50 s are observed during the growth process. Strong wall slip, metastable states, and transient nucleation of three-band flows are also reported and discussed in light of previous experiments and theoretical models.

DOI: 10.1103/PhysRevLett.93.018301 PACS numbers: 83.60.–a, 83.80.Qr, 47.50.+d, 43.58.+z

Wormlike micelle solutions exhibit strong shear-thinning behavior due to the coupling between their microstructure and the flow. Along the steady-state flow curve (shear stress σ vs shear rate $\dot{\gamma}$), a drop of up to 3 orders of magnitude in the effective viscosity $\eta = \sigma/\dot{\gamma}$ is observed in a very narrow stress range leading to a stress plateau [1]. Such a sharp transition made wormlike micelle solutions appear as a model system to study shear-induced effects in complex fluids. Indeed, in many systems featuring a shear-induced structure, the flow curve exhibits a stress plateau: as examples, let us mention emulsions in the vicinity of the yield stress [2], polymer solutions near the cloud point [3], concentrated surfactant solutions [4,5], liquid crystalline polymers [6], and entangled polymer solutions [7].

A partial understanding of the flow curve of wormlike micelles has emerged thanks to local scattering and velocimetry experiments. Above a critical shear rate $\dot{\gamma}_1$, a birefringent band normal to the velocity gradient occupies an increasing part of the gap as the shear rate is increased [8,9]. This shear-induced birefringent band was clearly identified as a nematic phase in the case of concentrated solutions and has a low viscosity compared to the isotropic phase [8,10]. Moreover, the velocity field was shown to separate into two differently sheared bands [11,12]: a weakly sheared region flowing at $\dot{\gamma}_1$ and a highly sheared region at $\dot{\gamma}_2$, the upper limit of the stress plateau. In the well-documented system CPCl/NaSal in brine [13], the equilibrium position δ of the interface between the two shear bands increases linearly with $\dot{\gamma}$ consistently with the "lever rule" according to which $\delta \propto (\dot{\gamma} - \dot{\gamma}_1)/(\dot{\gamma}_2 - \dot{\gamma}_1)$ [11].

This simple shear-banding scenario has been observed in other complex fluids [4]. Because of their generality, inhomogeneous flows have motivated many recent theoretical works involving phenomenological models [14] or microscopical approaches [15] that take into account the coupling between the flow and the microstructure of the fluid. Such models deal with the stability of the coexisting bands and, in some cases, suggest the existence of fluctuating or chaotic flows [16].

However, in order to fully validate these models, more experimental data are needed that show the kinetics of banding formation [9] and the temporal evolution of the inhomogeneous flows. In particular, due to the limited temporal resolution of current local velocimetry techniques [nuclear magnetic resonance (NMR) [12,17,18] and dynamic light scattering (DLS) [11]], a *time-resolved* description of the velocity field is still missing.

In this Letter, velocity profiles obtained in cylindrical Couette geometry by high-frequency ultrasonic velocimetry and recorded every 2 s *simultaneously* to global rheological data are presented for a startup experiment followed over about 6 h. For one of the much studied micellar systems [cetyl trimethyl ammonium bromide (CTAB) in D_2O], we show that two very different time scales are involved in the dynamics of shear banding. (i) A three-step nucleation and growth of a high-shear band occurs on a few hours. (ii) "Fast" oscillations of the band position with a period of about 50 s are pointed out. Subtle additional effects such as strong wall slip and transient nucleation of three-band flows are also reported and discussed.

We focus on the salt-free wormlike micelle solution made of CTAB at 20% wt. in deuterated water (D_2O) at a temperature of 44 °C, i.e., in the vicinity of the isotropic–nematic (I–N) transition that occurs at $T_{IN} = 39$ °C [8,17]. Rheological data are measured using a stress imposed rheometer (TA Instruments AR 1000) and a Couette cell of inner radius $R_1 = 24$ mm and gap width $e = 1.1$ mm. The cell is surrounded by a solvent trap containing water to prevent evaporation. Our local velocimetry technique is based on time-domain cross correlation of high-frequency ultrasonic signals backscattered by the moving fluid. Postprocessing of acoustic data allows us to record a velocity profile in 0.02–2 s with spatial resolutions of 40 μm in the velocity gradient direction and 60 μm in the vorticity and velocity directions (see Ref. [19] for more details). In order to enhance the scattering properties of our system, we add a small amount of colloidal particles (1% wt. polystyrene spheres of diameter 3 to 10 μm). We checked that the linear

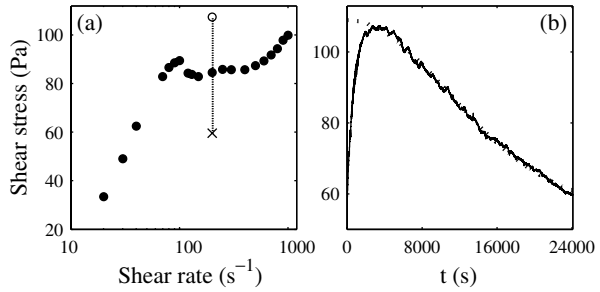

FIG. 1. (a) "Quasistatic" flow curve $\sigma(\dot{\gamma})$ obtained at $T = 44\,^{\circ}\mathrm{C}$ under controlled shear rate (15 min per data point) by averaging the shear stress over the last 100 s of each step. The dotted line corresponds to the stress response during a startup experiment at 186 s^{-1}. ○ and × symbols indicate, respectively, the maximum and the last value of σ. (b) Temporal response of the shear stress $\sigma(t)$ during a startup experiment at 186 s^{-1} (thin line). The thick dotted line is the sigmoidal relaxation with $\sigma_\infty = 56.4$ Pa, $\sigma_M = 109$ Pa, and $\tau_{ss} = 15\,450$ s (see text).

rheological properties as well as the plateau behavior were not significantly affected by the addition of those scatterers.

Using the shear rate imposed mode of the rheometer, we first apply increasing shear rates during a scanning time of 900 s per step. The resulting flow curve $\sigma(\dot{\gamma})$ shown in Fig. 1(a) presents a stress plateau at $\sigma^\star \approx 84$ Pa that extends from $\dot{\gamma}_1 \approx 50\ s^{-1}$ to $\dot{\gamma}_2 \approx 500\ s^{-1}$ corresponding to a drop in the effective viscosity by an order of magnitude. Note that, in the system under study, the features of the plateau ($\sigma^\star$, $\dot{\gamma}_1$, and $\dot{\gamma}_2$) depend dramatically on the scanning time as already reported in Ref. [8].

In the following, we apply a steplike shear rate into the plateau region from 0 to 186 s^{-1} at time $t = 0$ and we record simultaneously the shear stress response $\sigma(t)$ and the velocity profiles for about 6 h. As seen in Fig. 1(b), $\sigma(t)$ increases from 60 to 105 Pa in 2000 s, then remains nearly constant at 107 Pa for 2500 s, and finally decreases very slowly for the rest of the experiment. This ultraslow decrease may be well fitted by a sigmoidal function $\sigma(t) = \sigma_\infty + (\sigma_M - \sigma_\infty)\exp[(-t/\tau_{ss})^2]$ with $\tau_{ss} = 15\,450$ s and $\sigma_\infty = 56.4$ Pa [20]. We checked that this very long time scale cannot be attributed to any evaporation effect by measuring the weight fraction of the sample before and after shearing using thermogravimetric analysis.

Figure 2 gathers the full ultrasonic velocimetry data on a spatiotemporal diagram of the local shear rate $\dot{\gamma}(x, t)$ calculated from the velocity $v(x, t)$ as $\dot{\gamma}(x, t) = -(R_1 + x)(\partial/\partial x)[v(x, t)/(R_1 + x)]$. The abscissas correspond to time t and the ordinates to the radial position x inside the gap of the Couette cell with $x = 0$ ($x = e$) at the rotor (stator). This representation reveals that the flow field slowly evolves in time but also undergoes "fast" fluctuations [21]. By first looking at the velocity profiles averaged over at most 6 min, we may distinguish three different regimes (indicated by arrows on Fig. 2 and summarized in Fig. 3) along the slow stress relaxation.

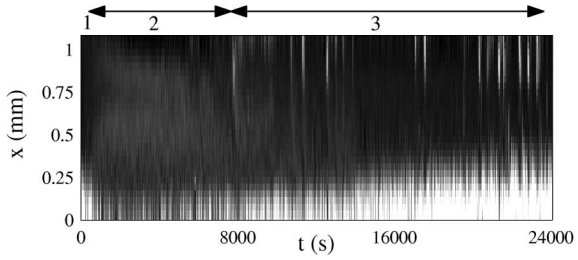

FIG. 2. Local shear rate $\dot{\gamma}(x, t)$. A linear gray scale is used: black and white correspond, respectively, to $\dot{\gamma} = 0$ and $\dot{\gamma} \geq 300\ s^{-1}$.

At the inception of the flow and for about 200 s, *two bands* bearing different shear rates, $\dot{\gamma}_h \approx 360$ and $\dot{\gamma}_l \approx 16\ s^{-1}$, coexist in the gap of the Couette cell [see ● symbols in Fig. 3(a)]. The interface between the shear bands is located at $\delta \approx 0.3$ mm from the rotor. Moreover, wall slip is present since the fluid velocity neither reaches the rotor velocity $v_0 = 200\ \mathrm{mm\,s^{-1}}$ at $x = 0$ nor perfectly vanishes at $x = e$. We define the slip velocities at the rotor v_{s1} and at the stator v_{s2} as the differences between the fluid velocity near the wall and the corresponding wall velocity, and get $v_{s1} \approx 79\ \mathrm{mm\,s^{-1}}$ and $v_{s2} \approx 3\ \mathrm{mm\,s^{-1}}$. Slip velocities are thus strongly dissymmetric and demonstrate that wall slip occurs preferentially in the low viscosity phase.

Second, after this first regime, the flow becomes *homogeneous* most of the time for about 8000 s [except for a very narrow region at the rotor, see Fig. 4(a)]. Strong wall slip is detected at the rotor ($v_{s1} \approx 138\ \mathrm{mm\,s^{-1}}$) while slip at the stator remains negligible [see ○ symbols in Fig. 3(a)]. Note that the sliding layer at the rotor supports a very high shear rate of about 3000 s^{-1} and thus unambiguously differs from a band of nematic phase thinner than our resolution of 40 μm (that would flow at $\dot{\gamma}_h$). Another striking feature of this velocity profile is the

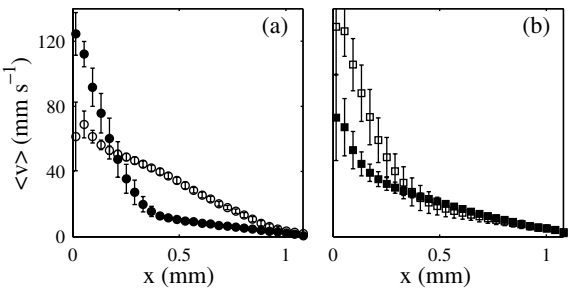

FIG. 3. Description of the slow dynamics. Velocity profiles $\langle v(x)\rangle$ averaged over (a) $t = 2$–25 (●), 4400–4700 (○), (b) 12000–12230 (■), and 23600–23840 s (□). The error bars are the standard deviations of these estimates. The rotor velocity at $\dot{\gamma} = 186\ s^{-1}$ is $v_0 = 200\ \mathrm{mm\,s^{-1}}$.

value of the "true" shear rate (calculated by removing the contributions of sliding layers) $\dot{\gamma}_{\text{true}} \approx 63\ \text{s}^{-1}$ for which the flow is expected to show (at least) two shear bands. This suggests that during this second regime, the system explores a metastable branch of the flow curve located above the stress plateau at $\sigma^\star$ [20].

Finally, from $t \approx 8000$ s until the end of the experiment, the velocity profiles show the *growth* of a low viscosity layer in the vicinity of the rotor [see Fig. 3(b)] qualitatively similar to the long time behavior reported in flow birefringence experiments [9]. This highly sheared band expands until it fills roughly one third of the gap. During this growth stage, the slip velocity v_{s1} decreases from 138 to 68 mm s^{-1} so that the local shear rate in the high-shear band $\dot{\gamma}_h$ remains roughly constant and equal to 360 s^{-1}. Moreover, the weakly sheared band bears a constant local shear rate $\dot{\gamma}_l \approx 30\ \text{s}^{-1}$. Thus, although the asymptotic state is still not perfectly reached, the interface position at the end of the experiment is compatible with the lever rule: $\delta = (\dot{\gamma}_{\text{true}} - \dot{\gamma}_l)/(\dot{\gamma}_h - \dot{\gamma}_l)e \approx 0.3$ mm.

Let us now get a closer look at the fast dynamics superimposed to the slow evolution described above. In the second regime ($t \approx 200$–8000 s), Figures 4(a) and 4(b) reveal that a thin band of width $\delta \lesssim 150\ \mu$m is nucleated and destroyed within short intervals of a few seconds unevenly every 5 to 20 s. When present, the band is sheared at $\dot{\gamma}_h$ and can be clearly distinguished from wall slip.

Moreover, Figs. 4(c) and 4(d) show that, during the expansion of the highly sheared band ($t \approx$ 8000–24 000 s), the interface is in fact subjected to periodic oscillations with a period of 50 s, while the slip velocity at the rotor never reaches a stationary value. As Fig. 5 points out, the slip velocity $v_{s1}(t)$ oscillates in phase opposition to the interface position $\delta(t)$, whereas the true shear rate $\dot{\gamma}_{\text{true}}(t)$ is synchronized with $\delta(t)$. Moreover, the temporal response of the shear stress recorded by the rheometer shows no obvious correlation with these oscillations [see Fig. 5(d)]. Thus, the classical rheological measurement $\sigma(t)$ does not allow one to detect the presence of the oscillatory behavior of the flow field.

These oscillations sometimes give way to the nucleation and destruction of a second highly sheared band at the stator [see Figs. 4(e) and 4(f)]. This phenomenon develops within roughly 200 s and takes place rather intermittently. On the spatiotemporal data $\dot{\gamma}(x, t)$, it shows up as a white patch for $x \gtrsim 0.8$ mm. This process seems to occur more frequently at the end of the experiment (see Fig. 2). Oscillations similar to those of Fig. 4(d) are clearly visible before and after the event of Fig. 4(f).

Let us finally discuss the origin of the various observed time scales. Concerning the *slow time scales*, our results are consistent with a nucleation and growth scenario

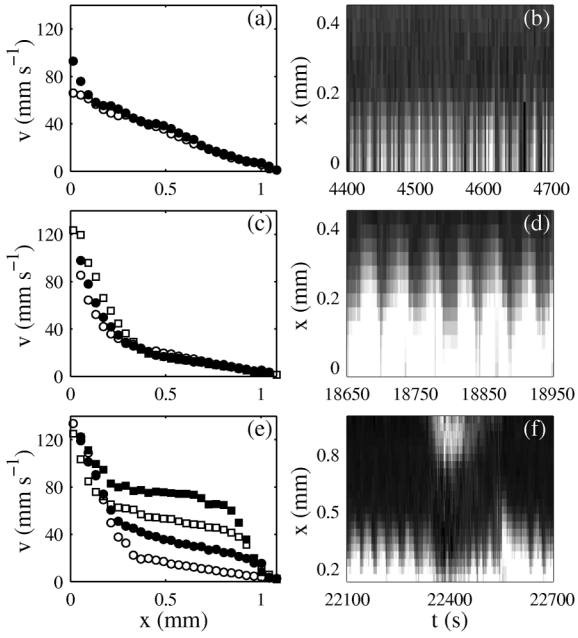

FIG. 4. Description of the fast dynamics. (a) Velocity profiles during the intermittent apparition of a highly sheared band at the rotor ($x \lesssim 150\ \mu$m) at $t = 4505$ (●), and 4508 s (○). (b) Enlargement of $\dot{\gamma}(x, t)$ over $t = 4400$–4700 s. (c) Velocity profiles during one interface oscillation at $t = 18800$ (○), 18 810 (●), and 18 818 s (□). (d) Enlargement of $\dot{\gamma}(x, t)$ over $t = 18\,650$–$18\,950$ s. (e) Velocity profiles during the nucleation of a second highly sheared band at $t = 22\,292$ (○), 22350 (●), 22 388 (□), and 22 463 s (■). (f) Enlargement of $\dot{\gamma}(x, t)$ over $t = 22\,100$–$22\,700$ s.

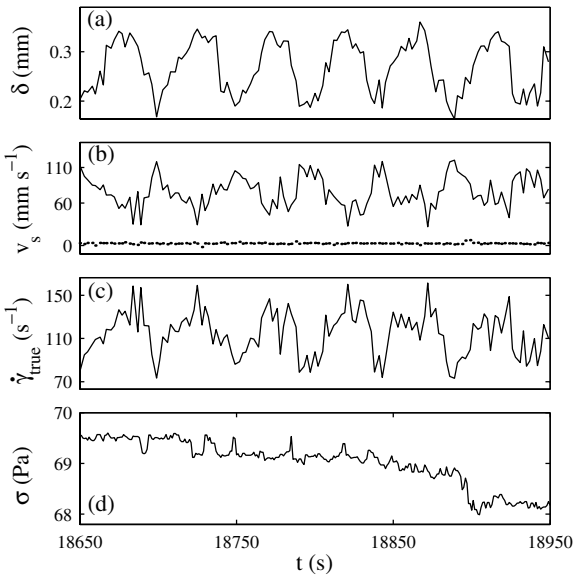

FIG. 5. Temporal fluctuations of (a) the position of the interface $\delta(t)$, (b) the slip velocities at the rotor $v_{s1}(t)$ (solid line) and at the stator $v_{s2}(t)$ (dotted line), (c) the true shear rate $\dot{\gamma}_{\text{true}}(t)$, and (d) the temporal response of the shear stress $\sigma(t)$ recorded during the oscillations of Fig. 4(d).

(although the first regime of Fig. 2 is not predicted by theoretical models) and reveal a strong similarity with the evolution reported in Ref. [9] on a CTAB/NaSal system. However, our system is more than 2 orders of magnitude slower: such a discrepancy could be explained by the differences in composition, electrostatic screening, or proximity to the *I–N* transition. Even though such microscopic details are not taken into account theoretically, existing works based on the Johnson-Segalman model provide a good description of the slow nucleation and growth mechanism [22,23].

Finally, the presence of *fast time scales* ranging from 5 to 200 s and thus strongly exceeding the micelle relaxation time $\tau_R \approx 40$ ms remains very puzzling [24]. Similar fluctuations have already been inferred from NMR velocimetry in the CPCl/NaSal micellar system [18], from DLS data in a lamellar phase [4], from rheological measurements in a concentrated suspension of silica beads [25] and in shear-thickening surfactant solutions [26], suggesting the presence of some general mechanism leading to such "fast" time scales.

Recent phenomenological models including dynamical equations for the micelle length and/or relaxation time predict oscillations and even chaoticlike states of the flow field that could be connected to the dynamics observed experimentally [16]. However, we believe that *wall slip dynamics* may play a major role in our experiments. Indeed, due to fluctuating slip velocities, the true shear rate is never stationary [see Fig. 5(c)] which could lead to the observed motion of the interface [23]. As a cause for the slip dynamics, one may invoke some multivaluedness of the shear rate inside the lubricating layers at a given shear stress, which would lead to an instability near the walls similar to stick-slip or "spurt" effect [27]. Further studies will focus on trying to isolate the bulk behavior from that of sliding layers and determine how the two are coupled.

In summary, our study reveals the existence of various dynamical regimes which are not fully captured by theoretical models that usually overlook the importance of wall-slip dynamics. We believe that a major issue for modeling inhomogeneous flows will be to include the two-dimensional nature of the flow near the walls, that may lead to fundamental differences from the bulk behavior. More generally, our results emphasize the need for time-resolved measurements in the study of complex fluid flows. Ultrasonic velocimetry allows a temporal resolution of about 1 s. Such a resolution is crucial since a wrong picture of the flow may be deduced from velocity profiles averaged on longer times with slower techniques.

The authors wish to thank D. Anache and the "Cellule Instrumentation" of CRPP for technical help with the experiment, and A. Aradian, F. Molino, P. Olmsted, G. Porte, and J.-B. Salmon for fruitful discussions.

*Corresponding author.
Electronic address: becu@crpp-bordeaux.cnrs.fr
†Present address: Rhodia Laboratoire du Futur, CNRS-FRE 2771, Bâtiment B de l'Institut Européen de Chimie et Biologie, 2 rue Robert Escarpit, 33607 Pessac Cedex, France.

[1] R. G. Larson, *The Structure and Rheology of Complex Fluids* (Oxford University Press, Oxford, 1999).
[2] P. Coussot *et al.*, Phys. Rev. Lett. **88**, 218301 (2002).
[3] G. Waton *et al.*, Macromolecules **37**, 2313 (2004).
[4] J.-B. Salmon *et al.*, Phys. Rev. E **68**, 051503 (2003); Phys. Rev. E **68**, 051504 (2003).
[5] L. Ramos, Langmuir **16**, 5846 (2000).
[6] C. Pujolle-Robic and L. Noirez, Nature (London) **409**, 167 (2001).
[7] P. Tapadia and S.-Q. Wang, Phys. Rev. Lett. **91**, 198301 (2003).
[8] E. Cappelaere *et al.*, Colloids Surf. A **104**, 353 (1995); Phys. Rev. E **56**, 1869 (1997).
[9] S. Lerouge *et al.*, Phys. Rev. Lett. **81**, 5457 (1998); Langmuir **16**, 6464 (2000).
[10] J.-F. Berret *et al.*, J. Phys. II (France) **4**, 1261 (1994); J.-F. Berret *et al.*, Eur. Phys. J. B **5**, 67 (1998); V. Schmitt *et al.*, Langmuir **10**, 955 (1994).
[11] J.-B. Salmon *et al.*, Phys. Rev. Lett. **90**, 228303 (2003).
[12] M. M. Britton and P. T. Callaghan, Phys. Rev. Lett. **78**, 4930 (1997); Eur. Phys. J. B **7**, 237 (1999).
[13] H. Rehage and H. Hoffmann, Mol. Phys. **74**, 933 (1991); J.-F Berret *et al.*, Phys. Rev. E **55**, 1668 (1997).
[14] G. Picard *et al.*, Phys. Rev. E **66**, 051501 (2002); J. K. G. Dhont, Phys. Rev. E **60**, 4534 (1999).
[15] P. D. Olmsted and P. M. Goldbart, Phys. Rev. A **41**, 4578 (1990); G. Marucci *et al.*, J. Non-Newtonian Fluid Mech. **21**, 329 (1986).
[16] S. M. Fielding and P. D. Olmsted, Phys. Rev. Lett. **92**, 084502 (2004); A. Aradian and M. E. Cates, cond-mat/0310660.
[17] E. Fischer and P. T. Callaghan, Europhys. Lett. **50**, 803 (2000); Phys. Rev. E **64**, 011501 (2001).
[18] R. W. Mair and P. T. Callaghan, J. Rheol. **41**, 901 (1997); W. M. Holmes *et al.*, Europhys. Lett. **64**, 274 (2003).
[19] S. Manneville *et al.*, cond-mat/0311072.
[20] C. Grand *et al.*, J. Phys. II (France) **7**, 1071 (1997); J.-F Berret and G. Porte, Phys. Rev. E **60**, 4268 (1999); J.-F. Berret *et al.*, Europhys. Lett. **25**, 521 (1994).
[21] Animations of the velocity profiles are available at http://www.crpp-bordeaux.cnrs.fr/~sebm/usv
[22] O. Radulescu *et al.*, Rheol. Acta **38**, 606 (1999).
[23] O. Radulescu *et al.*, Europhys. Lett. **62**, 230 (2003).
[24] A mechanical effect, such as a small amount of wobble, would lead to a single time scale corresponding to the rotation period 0.75 s of the rotor. Moreover, $\dot{\gamma} = 186\ s^{-1}$ is far from any hydrodynamic or elastic instability.
[25] D. Lootens *et al.*, Phys. Rev. Lett. **90**, 178301 (2003).
[26] R. Bandyopadhyay and A. K. Sood, Europhys. Lett. **56**, 447 (2001).
[27] J. L. A. Dubbeldam and J. Molenaar, J. Non-Newtonian Fluid Mech. **112**, 217 (2003).